Journal of Nanomedicine & Biotherapeutic Discovery

López et al., J Nanomedine Biotherapeutic Discov 2015, 5:4
DOI: 10.4172/2155-983X.1000137

Research Article Open Access

Histology Study of Wistar Rats Implanted With and Without C6 Cells and the Effect of NPt-Cu Nanoparticles

Tessy López[1,4*], Emma Ortiz Islas[2], Andrea Morales[2], José Luis Cuevas[1], Esteban Gomez[4], Joaquín Manjarrez[2], Patricia Guevara[2], Martha Lilia Tena[2], Aurora Sánchez[2], Pier Paolo Lottici[3], Danilo Bersani[3], Hugo Monroy[2] and Octavio Novaro[4,5]

[1]*Universidad Autónoma Metropolitana-Xochimilco, Nanomedicine Laboratory, Calzada del Hueso 1100, Villa Quietud, Coyoacán, 04960, D.F., México*

[2]*Instituto Nacional de Neurología y Neurocirugía "MVS", Insurgentes Sur 3877, La Fama, Tlalpan, 14269, D.F., México*

[3]*University of Parma, Physics and Earth Sciences Department, Parco Area delle Scienze, 7A, 43124 Parma, Italy*

[4]*Universidad Nacional Autónoma de México, Physics Institute, Theoretical Physics Department, Circuito de la Investigación Científica Ciudad Universitaria, 04510, D.F., México*

[5]*El Colegio Nacional, Donceles 104, Centro Histórico, D.F., México*

Abstract

In the present research, we prepare nanoparticles of Cu-TiO_2 using different copper precursors with a sol-gel technique. In these nanobiocatalysts, titania was functionalized on the surfaces with sulfates, fosfates and GABA. We used intracranial glioma the C6 cell method for evaluating the efficiency and toxicity of the glioblastoma multiforme (GBM) tumor. The nanoparticles were tested in four groups of Wistar rats. To wit: 1-reference (normal); 2- C6 cells only; 3- tumor model used with different copper complexes supported in TiO_2. The following subdivision were: 3a- tumor model used with $Cu(NH4)_2$ Cl_4 /F-TiO_2. 3b-Tumor model used with $Cu(Oac)_2$/F-TiO_2. 3c-Tumor model used with $Cu(acac)_2$/F-TiO_2. Finally, we add a 3d-titania reference. Immunohistochemical technique shows the following results: less inflammatory response as well as controlled gliosis. In addition a decrease in tumor size in each group.

Keywords: Catalytic nanomedicine; Copper complexes; C6 cell line; Functionalized nanoparticles; GBM; Histological features

Introduction

GBM represents 12–15% of all brain tumors and 50–60% of astrocytoma [1-4]. The key features of malignant glioma include: local invasive growth and strong angiogenesis [3]. Despite many advances in surgical and medical therapies in recent years, the clinical outcome of this disease is still dismal under the best available treatment regime. Several factors concur to make GBM treatment notoriously difficult [5,6]. First, the tumor cells through their rapid life cycle, becomes quite resistant to conventional therapies [7]. Current GBM treatments include surgery, radiation therapy, and chemotherapy, or a combination thereof, sometimes supplemented with novel therapies. Despite recent advances, survival of GBM patients remains quite limited. The invasive nature of GBM represents a major clinical challenge because it leads to poor outcomes. Invasion of GBM into healthy tissues restrict chemotherapeutic access and complicates surgical resection [8]. There are at least two factors that make GBM treatment extremely difficult. First, the brain has a limited capacity to repair itself. Second, GBM is a quickly mitotic tumor, highly invasive and resistant to therapies [9,10].

Cis-Platinum has been the most studied drug for cancer treatment. In the last few years tests have been conducted with functionalized platinum nanoparticles supported on titania (NPt-Pt) which, after several studies, are used mainly in patients with GBM brain tumor [11-14]. However, an important factor to consider is the very high cost of cis-Pt and others platinum compounds. In the present research, we tested the replacement of NPt-Pt by NPt-Cu nanoparticles [15,16] with encouraging results.

Microglia, which contribute substantially to the tumor mass of glioblastoma, have been shown to play an important role in glioma growth and invasion. While a large number of experimental studies in microglia in glioma provided evidence for their tumor-supporting roles, there also exist hints supporting their anti-tumor properties [17]. Microglial activities during glioma progression seem multifaceted [18-20]. It is necessary to use experimental neurooncology animal models to assess the efficiency of innovative approaches for the treatment of brain tumors [21,22].

In this work, the NPt-Cu 3a- tumor model used with $Cu(NH4)_2$ Cl_4 /F-TiO_2. 3b-Tumor model used with $Cu(Oac)_2$/F-TiO_2. 3c-Tumor model used with $Cu(acac)_2$/F-TiO_2 and 3d-titania reference, were characterized by Transmission Electronic Microscopy to establish the particle size obtained as well as Micro Raman spectra. Then cell viability is evaluated, we determine macroscopic analysis of a Wistar the rat brain with an implanted tumor, we then analyze histological features and the proliferation markers (proliferation cell nuclear antigen - PCNA, ki67) and the differentiation (glial fibrillary acidic protein, nestin, S-100, IDH1), in GBM models and treat them with copper nanoparticles supported in TiO_2.

***Corresponding author :** Tessy López, Universidad Autónoma Metropolitana-Xochimilco, Nanomedicine Laboratory, Calzada del Hueso 1100, Villa Quietud, Coyoacán, 04960, D.F., México, Tel: +525517960183; E-mail: tessy3@prodigy.net.mx

Received July 21, 2015; **Accepted** August 31, 2015; **Published** September 04, 2015

Citation: López T, Islas EO, Morales A, Cuevas JL, Gomez E, et al. (2015) Histology Study of Wistar Rats Implanted With and Without C6 Cells and the Effect of NPt-Cu Nanoparticles. J Nanomedine Biotherapeutic Discov 5: 137. doi:10.4172/2155-983X.1000137

Experimental Methods

Sample preparation

A biocompatible material was obtained by the functionalization of titania's surface with sulfates, phosphates and gamma amino-butyric acid (GABA). The functionalized-titania material was used as a carrier of copper complexes. The functional group precursors were sulfuric acid (REASOL, 95.98%), phosphoric acid (MONTERREY, 85%) and GABA (SIGMA ALDRICH, 1%). The material was prepared according to the following process previously reported by López T et al. [23]. The copper complexes used for this study were copper (II) monohydrated acetate [$Cu(Oac)_2$] (SIGMA-ALDRICH,99.99%) and copper (II) acetylacetonate [$Cu(acac)_2$] (ALDRICH, 99.99%). The amounts used were calculated to obtain the molar ratios of water:alkoxide 16:1 and ethanol:alkoxide 8:1. The amount used of each copper complex was 10% mol in TiO_2.

Procedure

The adequate amount of copper complex was dissolved in a mixture of ethyl alcohol and deionized water. Meanwhile, GABA was dissolved in deionized water. After that, both solutions were mixed and refluxed at 70°C under constant stirring. After this stage, sulfuric and phosphoric acid were added to the reactor's synthesis. The final solution was refluxed at 70°C for 24 h. The water and alcohol excess removal, as well as the drying of the samples were done in the same way as in the functionalized titania (F-TiO_2) sample. 3a- tumor model used with $Cu(NH_4)_2$ Cl_4 /F-TiO_2. 3b-Tumor model used with $Cu(Oac)_2$/F-TiO_2. 3c-Tumor model used with $Cu(acac)_2$/F-TiO_2 and 3d-titania reference. The particle sizes of the samples were measured using TEM. Micrographs were obtained using a JEOL JEM-2100F electron microscope with a 200 kV accelerated electron beam. The samples were placed over a copper grid with a holey carbon support film for F-TiO_2 and a gold grid with a holey carbon support film the other samples.

Characterization

Cell culture and *in vitro* cell viability test: The COS-7 fibroblast-like cell line derived from monkey kidney tissue obtained from the American Type Culture Collection (ATCC) were grown in Dulbecco´s Modified Eagle´s Medium (DMEM; Invitrogen Life Technologies-GIBCO, Carlsbad, CA, USA) supplemented with 10%(v/v) fetal bovine serum (FBS; Invitrogen Life Technologies-GIBCO), 100 U/mL penicillin, 100 µg/mL streptomycin, and maintained under humidified atmosphere of 5% CO_2 at 37°C. The cells were treated for 8 hours with each different concentration (0.01, 0.05 and 0.1 mg/mL) of TiO_2 (as a negative control) and $Cu(acac)_2$/F-TiO_2 diluted in serum free DMEM.

The cell viability after treatment with the materials was evaluated by using the MTT (3-4, 5-dimethylthiazol-2-yl)-2,5-diphenyl tetrazolium bromide (SIGMA ALDRICH, St. Louis, MO, USA) assay, which determines the ability of healthy cells to produce formazan from the cleavage of the tetrazolium ring of MTT directly indicating proper cellular mitochondrial activity. Briefly, ELISA plates with cells treated with nanoparticles of Cu-TiO_2, were washed with a fresh culture medium and then incubated in a fresh medium containing MTT (0.5 mg/mL) for 3 h at 37°C. The MTT medium was discarded and the cells were incubated in dimethyl sulfoxide (DMSO) to dissolve the formazan aggregates. The intensity of the MTT products was read at 570 nm by using an ELISA microplate reader (iMark, Bio-Rad Laboratories Inc., Hercules, CA, USA). Each experiment was performed in triplicate. Data were normalized to untreated control and analyzed with software GraphPad Prism ver. 4.0.

Immunocytochemistry and microscopy: For double labeling immunofluorescence, the cells were fixed with 2% paraformaldehyde in Phosphate Buffer (PBS) at room temperature (RT) for 15 min and permeated in 0.1% Triton X-100-PBS (PBS/T). After blocking for 1 h. at RT (0.5% gelatin and 1.5% fetal bovine serum in PBS), cells were incubated for 1 h. at RT in a humidity chamber with antibody anti-α-tubulin monoclonal-IgG (Santacruz Biotechnology). The corresponding secondary antibodies to mouse-IgG were tagged with fluorescein-isothiocyanate (FITC) (Jackson Immuno-Research Laboratories, Inc. West Grove, PA, USA), and incubated in PBS/T for 1 h. at RT (1:1000 dilution) and the actin cytoskeleton was stained with the dye Rhodamine-Phalloidin (Molecular Probes, Invitrogen Life Technologies Grand Islands, NY, USA). In experiments with cells, in vivo labeling was done by including the fluorescent mitochondrial marker MitroTracker Deep Red (Molecular Probes). Immunolabeled cells were analyzed by epifluorescence through 60x (numerical aperture (NA):1.00 W) and a 100x (NA: 1.3 Oil) Plan-Fluor Lens coupled to a Nikon Eclipse-80i Microscope (Nikon Corp., Tokyo, Japan). The images were obtained and recorded by using a Nikon digital sight-DG-Ri1 camera controlled with the Nikon NIS-Elements AR-3.0- SP7 software included in the system (Nikon Corp).

Micro-Raman spectroscopy: Non-polarized Raman spectra on the powdered samples were recorded at 632.8 nm in a nearly backscattered geometry with a Horiba-Jobin Yvon LabRam micro-spectrometer (300 mm focal length spectrograph) equipped with a Peltier-cooled CCD detector and an integrated Olympus B40x microscope. The spectral resolution was about 1.5 cm^{-1}.

The Rayleigh radiation was blocked by an edge filter and the backscattered Raman light was dispersed by an 1800 grooves/mm holographic grating on a Peltier cooled CCD, consisting of an array of 1024/256 pixels. The entrance slit-width was fixed at 100 µm. The laser power was adjusted by means of density filters to avoid uncontrolled thermal effects. The potential on the sample was always less than 0.2 mW.

Spectra were collected using long working distance 50x microscope objectives. Typical exposures were 10-60 s, with 5-9 repetitions. The system was calibrated using the 520.6 cm^{-1} Raman band of silicon or by means of crystalline references. The data analysis was performed by LabSpec built-in software.

Rat C6 Glioma cell cultures: Rat C6 glioma cell line was obtained from the European Collection of Animal Cell Cultures (Porton Down, UK). The cells were grown in 60-mm Petri dishes in an F-12 Ham Nutrient Mixture supplemented with 10% FBS Gold serum, 2 mM glutamine, 100 U/ml penicillin, and 100 µg/ml streptomycin in a humidified atmosphere of 95% air and 5% CO_2 at 37°C. For subcultures, cells were harvested in trypsin–EDTA solution twice a week and seeded at a density of 10^6 cells per dish. For experimentation, eight and 20 passage cells were used.

Preparation of C6 glioma cell for GBM model: C6 glioma cells (seeded at a density of 30,000 cells/well) were grown in 96-well plates in standard culture conditions. Twenty-four hours before exposing cells to the selected chemicals, the culture medium was replaced with a fresh serum-free medium. Cell viability and mitochondrial function were measured by 3-(4,5-dimethyl-2-thiazolyl)-2,5-diphenyl-2H-tetrazolium bromide (MTT) reduction to MTT formazan by cellular mitochondrial dehydrogenases. Following exposure to orexin A and orexin B for 24 and 48 h, the cell cultures were washed in PBS before the addition of MTT (0.5 mg/ml) and incubated for 3 h at 37°C. Formazan

crystals were solubilized in dimethyl sulfoxide (DMSO; 100%) and absorbance proportional to the number of viable cells were measured at 570 nm using a microplate reader (EnVision 2103, PerkinElmer).

Implantation of tumor cells in the rat brain: The Wistar adult male rats (180–250 g) maintained on a 12:12 light/dark cycle with food and water ad libitum were intraperitoneal anesthetized with ketamine-xylazine (80/10 mg/kg) response. 1×10^6 cells were trypsinized, washed twice, suspended and diluted in a volume of 2 µL of DMEM (non FBS) and were slowly injected during a 2 min. period using an injection cannula (25-gauge) (Hamilton Co., Reno, NV).

The rats were returned to the animal facility after recovery from anesthesia. Each rat was weighted every other day in the first two weeks and every day after, and was evaluated for neurological deficits started at 1 week after the implantation. Abnormal behaviors and neurological signs associated with brainstem tumor were observed everyday started at 1 week after C6 cells implantation, and onset of paresis was recorded. A modified rotator test was used to assess coordinated motor function. Nanoparticles were applied three weeks later since the abnormal behavior and neurological signs. The rats were divided in groups and maintained in the vivarium conditions until they were sacrificed.

Tissue preparation for histological studies: Two weeks after treatment, mice were anesthetized with chlorohydrate and perfused transcardially with 4% paraformaldehyde in PBS. Whole brains were removed and postfixed overnight in 4% paraformaldehyde in PBS. The brains were coronally sectioned into 5 slices, and these were embedded in paraffin. Ten-micrometer-thick tissue sections were cut and stained with hematoxylin-eosin reagent. Histological variables were identified for each group: necrosis, macrophages, inflammatory cells, lymphocytes, hemorrhage; presence of nanoparticles, vessels and astrocytes, also the boundary of the tumor was evaluated.

Results and Discussion

In Figure 1 (A) a high intensity peak at 230 cm^{-1} is observed in the samples of $[Cu(NH_4)_2Cl_4{\cdot}2H_2O]$/F-$TiO_2$ and $CuCl_2$/F-TiO_2 characterized by carbon-oxygen bindings of GABA. Here we can notice the strong bonds between GABA and TiO_2.

Also in these spectra we have three peaks represented at 400, 514 and 636 cm^{-1}, respectively. The first one is caused by the presence of nitrogen-hydrogen bonds and the rest are caused by the bonds with Cl. Later, the spectra continue as a flat line because no bonds are formed between TiO_2 and –OH radicals. In the $Cu(Oac)_2$/F-TiO_2 spectra, we can see a peak at 500 cm^{-1}, due to C-O bonds followed by a flat line.

In the $Cu(acac)_2$/F-TiO_2 we can observe a peak at 470 cm^{-1}, caused by a Raman tension vibration of bonds Ti-O-Ti. At 1250 cm^{-1}, we can find an energy gap caused by carbonyl bonds C-O. At 2930, 3000 and 3050 cm^{-1} we can observe peaks corresponding carboxyl bonds C=O.

At 230 cm^{-1} a peak is only observed in the samples with Cl^-. Thenceforth three peaks appear at 400, 514 and 536 cm^{-1}, caused by the N-H bonds of GABA. Finally, we observe a flat line. The Raman spectra of a dried gel obtained Figure 1 (A) had features typical of the anatase phase. The dried gel obtained using oxalic copper had a complex Raman spectrum, Figure 1 (B) which cannot be ascribed to a TiO_2 phase even if coordination compounds of the oxalic acid are likely. Bonds of the oxalic copper with the titania network are stronger.

In vitro cell-toxicity test

After 8 h of treatment (Figure 2), we observed that material $Cu(acac)_2$/F-TiO_2 induced 20% apoptosis to the minimum concentration of 0.01 mg/mL. However, at maximum concentration the materials induced cell death (between 70% and 80%), compared with their respective control (TiO_2) which only induces 10% of cell death at the same concentration.

To determine whether the presence of both materials induced changes in the cellular cytoskeleton, we analyzed the integrity of the cytoskeleton of actin and tubulin after 8 hours of incubation with the maximum concentration of material (0.1 mg/mL). With the purpose to recognize the tubulin cytoskeleton (anti-α-tubulin) and a specific dye for fibrillar actin (phalloidin-rhodamine) an antibody is used.

In Figure 3 we show the bright field in the crystals formed by the materials in the green channel and the radial structure of the tubulin cytoskeleton, which parts of a microtubule-organizing center, a structure of fibrillar actin in the red channel in cells, in control the structure remains normal in both materials (TiO_2).

In contrast, the $Cu(acac)_2$/TiO_2 material causes the rupture microtubules center structure by switching it to a structure surrounding the nucleus. This produces a total degradation of actin filaments (see arrowhead). This result clearly indicates that copper nanoparticles supported in F-TiO_2 induce an alteration of the cytoskeletal structure.

The mitochondria play a critical role in the generation of metabolic energy trough Krebs cycle in the cells. Recently it has been reported that the DNA development in the mitochondria via telomeres using as enzymatic catalyst the telomerase [24]. This establishes that mitochondria are not unitary structures; otherwise, they form a mitochondrial network around the nucleus, and propagate throughout the cell cytoplasm.

Recent research have established that the alteration of the shape of mitochondria reflects induction of stress, changes in the redox state and apoptosis [24]. Therefore, we have analyzed the $Cu(acac)_2$/F-TiO_2 provoking cytotoxicity and very high alterations in mitochondrial shape.

In Figure 4, staining with MitoTracker Deep Red dye is shown with metabolically active mitochondria. In the control, we observed the normal shape of the mitochondria. In the incubated cells with the nanobiocatalyst $Cu(acac)_2$/F-TiO_2 the mitochondrial network was lost. The $Cu(acac)_2$/F-TiO_2 was concentrated in the surrounding nucleus and also presents a more elongated morphology than most fibers.

Statistical analysis

Data are presented as median. Independent experiments were pooled when the coefficient of variance could be assumed identical.

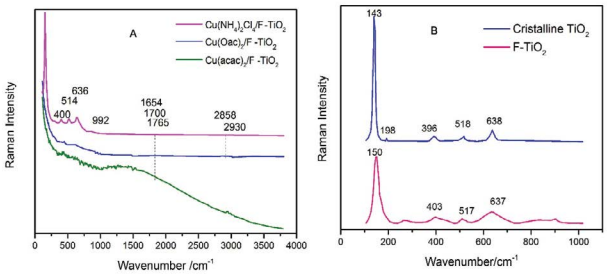

Figure 1: (A) Raman intensity of copper complexes in F-TiO_2, NPt-Cu. (B) Raman intensity differences between crystalline TiO_2 and the F-TiO_2 with SO_4-, PO_4- and GABA.

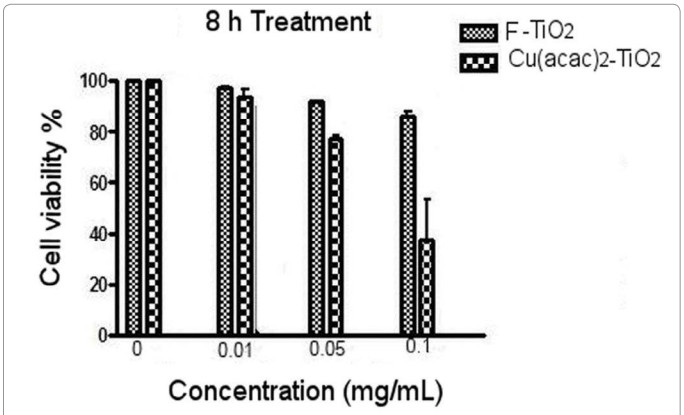

Figure 2: Cell viability induced by TiO2 and Cu(acac)2/F-TiO2 during 8 hours.

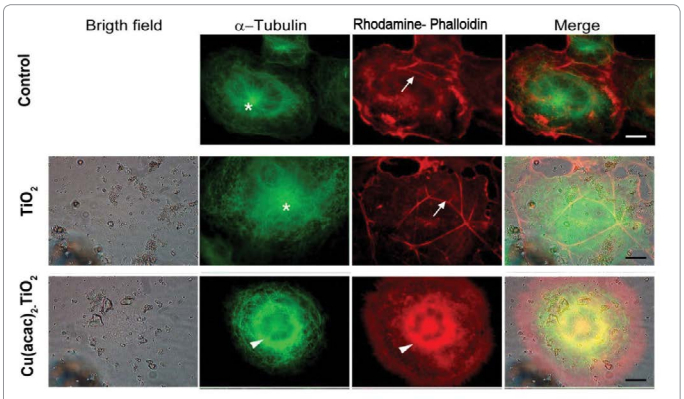

Figure 3: The Cu(acac)2/F-TiO2 material induces alterations in the structure of the cytoskeletal organization.

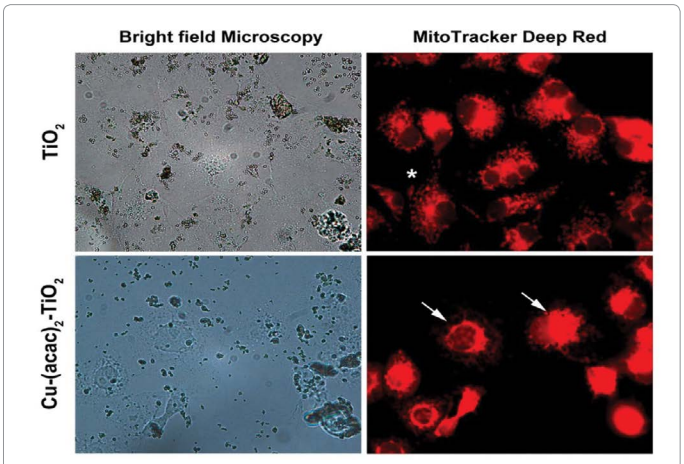

Figure 4: Mitochondrial network damaged by the Cu(acac)2/F-TiO2 which is concentrated in the surrounding nucleus. Presence of elongated morphology.

One-way ANOVA was used to analyze the effects of group. $P<0.05$ was considered statistically significative.

Histopathological findings

In the normal groups, any damage was observed. In the tumor group treated with $Cu(acac)_2/F\text{-}TiO_2$ necrosis areas, hemorrhagic zones, inflammatory infiltrates, mitosis figures, stockades were evidenced. Complete nanoparticles surrounded and without any response in the periphery zone were observed. Also, they were highly characterized by peritumoral gliosis, with more presence of machrophagic cells, with low quantities of tumor cells. We notice an inflammatory infiltration. In the groups that contain the nanobiocatalysts, the tumor is reduced, and the inflammatory response by macrophage cells and reactive gliosis is augmented (Figure 5).

In Table 1 we show the immunohistochemistry results. The tumor was positive immunoreactive to GFAP, vimentin, nestin, P53, IDH, S-100. TNFα, fasin, NGF, and was negative to α-integrin, CD200. Iba1, CD68 and in Table 2 we show the immunohistochemical results of the boundary of the tumor.

In the second group (tumor presence) there is low reactive inflammatory response by astrocytes and microglia, however in the third group we noticed more necrosis, hemorrhagic zones and more presence of nanoparticles. The immunoreaction was negative for most of the primary antibodies used. In the 3a group the primary antibodies expression was elevated in relation to other groups.

In the 3c group loss of primary antibodies expression and smaller tumoral size, but more inflammatory and gliosis expression were observed. Figure 6 shows a histogram according the different histological findings by each group.

GBM accounts for 12–15% of all brain tumors and 50–60% of astrocytomas [7]. The average survival time of GBM is less than 1 year from diagnosis, which makes it a considerable public health issue [4,25].

Conventional GBM therapies consist of surgery, radiotherapy, and chemotherapy or a combination of these [2]. Current chemotherapeutic strategies for tumors of the Central Nervous System are largely ineffective. This is due, in part, to the lack of drug delivery systems for the central nervous system. Recurrence usually means the tumor is becoming more aggressive, genetically and clinically, and it has acquired resistance to the adjuvant therapy [26].

Temozolomide (TMZ) is the primary chemotherapeutic agent by oral administration for treatment of GBM. It has a fast rate of degradation under physiological conditions, but it has poor penetration of the blood-brain barrier and cellular absorption. Major challenges in GBM treatment are drug delivery across the blood-brain barrier, restriction of damage to healthy brain tissues, and limitation of resistance to therapies. The blood–brain barrier hinders the passage of systemically delivered therapeutics, and the brain extracellular matrix limits the distribution and longevity of locally delivered agents, the FDA has 5 chemoterapeutic agents for control release from reservoirs made of several nanoparticles. In general, organic nanoparticles are biodegradable [18,27].

Our optimal therapeutic agent for brain tumors would selectively cross the blood-brain barrier, could be accumulated in the tumor tissue and be activated from an innocuous nanobiocatalyst within the tumor. The nanobiocatalyst should be effective in treating intracranial tumors. The nontoxic, tumor-specific targeting properties of the nanobiocatalyst system make it safe and low cost [28]. On the other hand, nanobiocatalysts, which act by breaking the C-C and C-N bonds in the tumor cell, can condition DNA/mitochondrial rupture (Figure 7).

The cellular signaling pathways important for the brain tumor genesis are multiple, with feedback mechanisms that can dramatically affect the efficiency of molecularly targeted therapeutic strategy [29].

Primary Antibodies	1	2	3a	3b	3c
GFAP	3	2	2	2	1
GFAPδ	1	2	2	3	0
Vim	2	2	2	3	1
S-100	3	1	2	2	1
Nestin	1	2	3	2	1
IDH1	3	0	1	1	0
P53	2	1	1	1	0
Alfa integrin	2	1	1	1	0
AQ4	1	1	3	1	0
NGF	1	0	3	1	0
CD200	1	1	2	1	0
Iba1	1	0	3	1	0
CD68	1	0	3	2	1
Fascin	1	0	3	2	1
IL6	1	0	3	2	1
IFI1	1	0	3	2	1
PCNA	25	10	8	7	2
KI67	18	10	5	5	1

Table 1: Immunohistochemistry results in GBM tumor. 1-C6 cells, 2- -tumor model used only with TiO_2, 3a,3b,3c- tumor model used with different copper complexes supported in TiO_2.

Histological Findings	1	2	3a	3b	3c
Tumoral necrosis	3	1	1	N	N
Tumoral inflammation	2	1	2	3	1
Macrophages presence	1	1	2	3	1
Lymphocytes presence	1	1	2	3	1
Vessels presence	2	1	2	2	1
Hemorrhage	2	2	1	N	N
Mitosis index	10	7	5	3	1
Nanoparticles	N	3	2	1	1
Peritumoral necrosis	N	1	2	1	N
Peritumoral inflammation	N	1	3	2	N
Peritumoral macrophages	N	1	2	3	1
Lymphocytes	1	1	2	2	1
Gliosis	1	1	3	3	1
Peritumoral hemorrhage	N	2	N	N	N
Nanoparticles	N	1	2	1	1
Neoplastic cells	N	1	2	N	N

Table 2: Histopathological findings in the GBM tumor and peritumoral boundary. 1-C6 cells, 2-tumor model used only with TiO_2, 3a,3b,3c- tumor model used with different copper complexes supported in TiO_2.

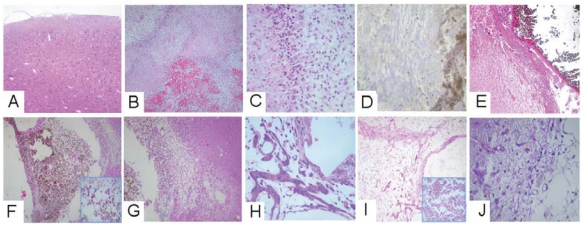

Figure 5: Histopathological findings. (a) Normal cortex, (b) now tumor shows pleomorphic astrocytes, (c) nuclear pleomorphism, with mitotic activity center necrosis around the vessels. In group (3a) are observed: (d) dense deposition of the nanoparticles and (f) tumor around those particles. In group (3b) are evidenced: (g) abundant macrophages immersed in nanoparticles and (h) the peritumoral area with edema and gliosis. In group (3c) (i) the tumoral areas, that the scarce neoplastic astrocytes are immersed in edema and vessels, in other areas are presented polimorfonuclear leucocytes with necrosis and in (j) we show inflammatory cells and gliosis.
3a- tumor model used with $Cu(NH_4)_2$ Cl_4 /F-TiO_2. 3b-Tumor model used with $Cu(Oac)_2$/F-TiO_2 .3c-Tumor model used with $Cu(acac)_2$/F-TiO_2.

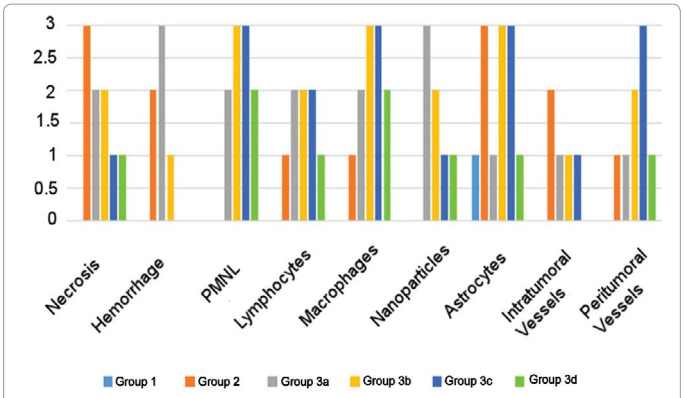

Figure 6: Histogram according to the different histological findings by each group.

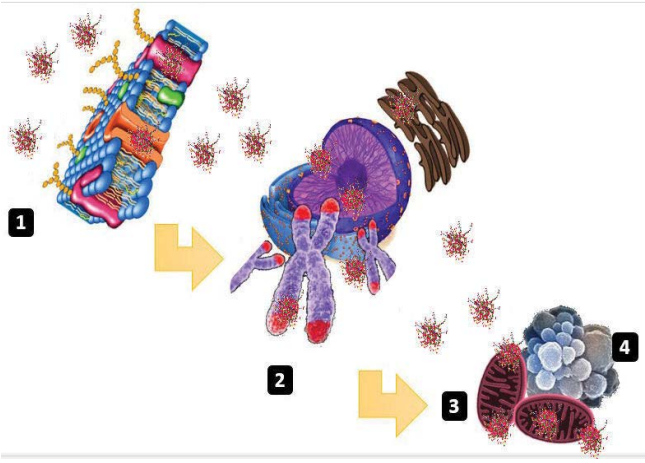

Figure 7: (1) Copper complexes in F-TiO_2 recognized by cell membrane, (2) copper complexes introduction provoking DNA rupture and (3), (4) mitochondrial rupture conditioning cell apoptosis.

The heterogeneous composition of human high grade gliomas, which consists of tumor stem cells and differentiated tumor cells with varying characteristics, further complicates their susceptibility to treatment [28].

The cell line C6 is a continuous cell line of rat glioma and, as a transplantable line, is frequently used for induction into *in vivo* model of primary brain tumor. It is believed that, pursuant to its histological traits and biological behavior, this experimental tumor corresponds to human anaplastic astrocytoma of grade II/III, which is characterized by proliferative and invasive potency, and marked cell differentiation. The C6 glioma has been used extensively for a variety of studies, but since it arose in a outbred Wistar rat, it is not syngeneic to any inbred strain, and its potential to evoke an alloimmune response is a serious limitation [21].

Despite this limitation, the C6 glioma model continues to be used for a variety of studies related to brain tumor biology [22]. These have included studies on growth, invasion, migration, BBB disruption, neovascularization, growth factor regulation and production, and biochemical studies [27].

Single-cell clonal analysis has revealed that C6 cells also have cancer stem cell-like characteristics, including self-renewal, the potential for multi-lineage differentiation in vitro and tumor formation *in vivo* [10,30].

IDH1/2 mutant gliomas harbor a distinct CpG island methylation profile (G-CIMP) that may promote the initiation and progression of secondary pathway gliomas by silencing tumor suppressive genes [31].

Within a glioma, microglia/macrophages make up the largest population of tumor-infiltrating cells, contributing at least one third of the total tumoral mass [32,33]. These glioma-infiltrating microglia/macrophages (the macrophage phenotype may predominate) are present in both intact glioma tissue and necrotic areas and their density in gliomas is positively correlated with glioma grade and invasiveness. There is compelling evidence that microglial cells are involved in creating a microenvironment that favors glioma growth [20,34] specifically, glioma invasion and the establishment of an immunosuppressive milieu are facilitated by the presence of intratumoral microglia [10].

The initial actions of glioma-infiltrating microglia, as the resident macrophages of the CNS, would be expected to be migration to the tumor site for rescue and display of properties similar to peripheral macrophages, such as phagocytosis, antigen presentation, and release of cytokines/chemokines as well as cytotoxins [35,36]. However, this microglia lost their phagocytic properties when in longer contact with glioma cells. In addition, microglia in glioma release interleukin (IL)-10, which helps to create an immunosuppressive microenvironment [17]. Even the armament of microglia is tactically employed by glioma cells to facilitate their survival, growth, and spread [35,37,38].

Copper complexes in functionalized titania, can regulate the expression of microglia environment and cytokines expression. They facilitate the inflammation and gliosis.

Also, its known signal transducer and activator of transcription protein (STAT)3 is a member of a transcription factor family, which is encoded by the STAT3 gene in humans [39-41]. STAT3 activation causes expression of genes that play important roles in mediating the signals of cytokines, mitochondrial pathways [41] and growth factors involved in cell growth [42], proliferation, differentiation , and apoptosis [43,44]. Copper complexes in functionalized titania conditions microtubules and mitochondrial disorganization and also DNA rupture producing cell apoptosis. In Figure 8, we suggest the action mechanism of copper complexes in F-TiO_2.

The Electron Transmission Microscopy was used to determine the particle size of the nanostructured samples, as shown the Figure 9. In this figure, we can observe that the nanoparticle sizes are between 1 and 5 nm. Furthermore, the first three figures show high crystallinity, while the F-TiO_2 in the last figure is clearly amorphous. Copper induces an organizing effect shown in the samples containing crystalline TiO_2-anatase.

Conclusions

It is well known that it is necessary to use experimental neurooncology animal models to assess the efficiency of innovative approaches for the treatment of brain tumors. Copper nanoparticles in functionalized titania seems to be an attractive and effective treatment for malignant gliomas. We conclude copper complexes supported in titania in rather low concentrations can actually decrease tumor size, can regulate antibodies expression, inflammatory and gliosis, which may prove quite beneficial for GBM treatment, rather than using chemotherapeutic drugs which may have harmful effects.

Acknowledgments

Thanks to CONACYT-México, IFUNAM, SECITI for the financial support.

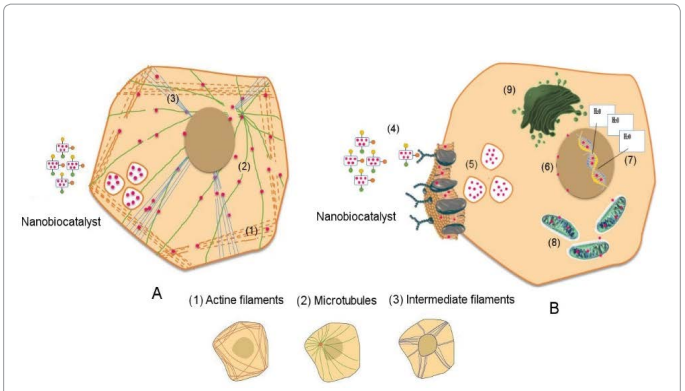

Figure 8: (a) Citoesqueletal disorganization caused by Cu-F/TiO_2 nanoparticles in tumor cells conditioning cell apoptosis. (b) Representation nanobiocatalyst (Cu/F-TiO_2) action in tumor cells, where the numbers from (4) to (9) represent the nanoparticules entry, transportation, entry by the nuclear pores, DNA rupture in hydrogen bonds, Mithocondrial rupture action and apoptosis induction conditioned by lisosomal degradation, respectively.

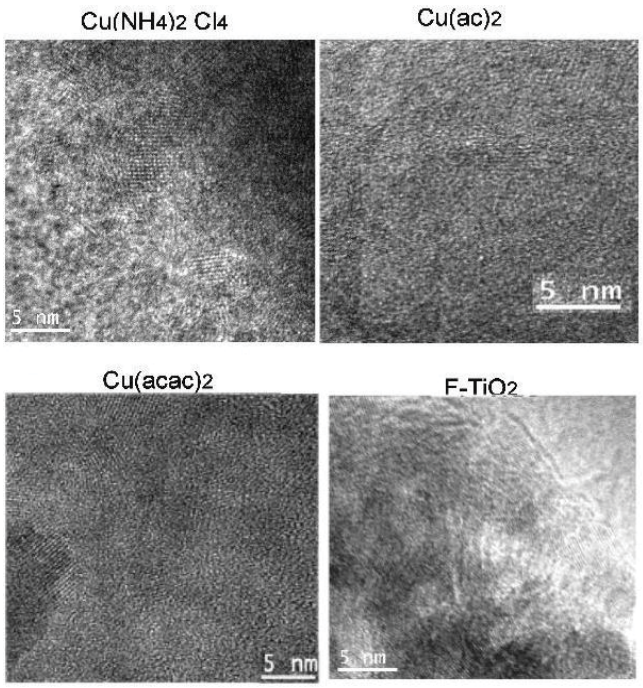

Figure 9: Transmission Electron Microscopy of the samples labeled as: Cu(NH4)2 Cl4,Cu(ac)2, Cu(acac)2,F-TiO2.

References

1. Inda MM, Bonavia R, Seoane J (2014) Glioblastoma multiforme: A look inside its heterogeneous nature. Cancers (Basel) 6: 226-239.
2. Ohka F, Natsume A, Wakabayashi T (2012) Current trends in targeted therapies for glioblastoma multiforme. Neurol Res Int 2012: 878425.
3. Patrick Y, Wen MD, Santosh K (2008) Malignant gliomas in adults. The New England Journal of Medicine 359: 492-507.
4. Louis DN, Ohgaki H, Wiestler OD, Cavenee WK, Burger PC, et al. (2007) The 2007 WHO classification of tumours of the central nervous system. Acta Neuropathol 114: 97-109.
5. Nakada M, Kita D, Watanabe T, Hayashi Y, Teng L, et al. (2011) Aberrant signaling pathways in glioma. Cancers (Basel) 3: 3242-3278.

6. Cancer Genome Atlas Research Network (2008) Comprehensive genomic characterization defines human glioblastoma genes and core pathways. Nature 455: 1061-1068.

7. Iacob G, Dinca EB (2009) Current data and strategy in glioblastoma multiforme. J Med Life 2: 386-393.

8. Rape A, Ananthanarayanan B, Kumar S (2014) Engineering strategies to mimic the glioblastoma microenvironment. Adv Drug Deliv Rev 79-80: 172-83.

9. Brandes AA, Tosoni A, Franceschi E, Reni M, Gatta G, et al. (2008) Glioblastoma in adults. Crit Rev Oncol Hematol 67: 139-152.

10. Shen G, Shen F, Shi Z, Liu W, Hu W, et al. (2008) Identification of cancer stem-like cells in the C6 glioma cell line and the limitation of current identification methods. In Vitro Cell Dev Biol Anim 44: 280-289.

11. Jo DH, Kim JH, Son JG, Song NW, Kim YI, et al. (2014) Anti-angiogenic effect of bare titanium dioxide nanoparticles on pathologic neovascularization without unbearable toxicity. Nanomedicine 10: 1109-1117.

12. Lopez T, Ortiz-Islas E, Guevara P, Gómez E (2013) Catalytic nanomedicine technology: Copper complexes loaded on titania nanomaterials as cytotoxic agents of cancer cell. Int J Nanomedicine 8: 581-592.

13. López T, Figueras F, Manjarrez J, Bustos J, Alvarez M, et al. (2010) Catalytic nanomedicine: A new field in antitumor treatment using supported platinum nanoparticles. In vitro DNA degradation and in vivo tests with C6 animal model on Wistar rats. Eur J Med Chem 4: 1982-1990.

14. Pison U, Welte T, Giersig M, Groneberg DA (2006) Nanomedicine for respiratory diseases. Eur J Pharmacol 533: 341-350.

15. Lopez T, Bosch P, Moran M, Gomez R (1993) Pt-SiOz Sol-Gel Catalysts: Effects of pH and Platinum Precursor. J Phys Chem 97: 1671–1677.

16. Asomoza M, Lopez T, Zamalloa A, Gomez R (1992) Catalytic Activity and Characterization of Pt-SiO2 Catalysts prepared by the Sol-Gel Method. New J Chem 16: 959-963.

17. Wu A, Wei J, Kong LY, Wang Y, Priebe W, et al. (2010) Glioma cancer stem cells induce immunosuppressive macrophages/microglia. Neuro Oncol 12: 1113-1125.

18. Liu L, Eckert MA, Riazifar H, Kang DK, Agalliu D, et al. (2013) From blood to the brain: Can systemically transplanted mesenchymal stem cells cross the blood-brain barrier? Stem Cells Int 2013: 435093.

19. 19.Li W, Graeber MB (2012) The molecular profile of microglia under the influence of glioma. Neuro Oncol 14: 958-978.

20. Graeber MB, Scheithauer BW, Kreutzberg GW (2002) Microglia in brain tumors. Glia 40: 252-259.

21. Barth RF, Kaur B (2009) Rat brain tumor models in experimental neuro-oncology: The C6, 9L, T9, RG, F98, BT4C, RT-2 and CNS-1 gliomas. J Neurooncol 94: 299-312.

22. Karmakar S, Olive MF, Banik NL, Ray SK (2007) Intracranial stereotaxic cannulation for development of orthotopic glioblastoma allograft in Sprague-Dawley rats and histoimmunopathological characterization of the brain tumor. Neurochem Res 32: 2235-2242.

23. López T, Ortiz E, Guevara P, Gómez E, Novaro O (2014) Physicochemical characterization of functionalized-nanostructured-titania as a carrier of copper complexes for cancer treatment. Materials Chemistry and Physics 146: 37-49.

24. Blackburn EH, Greider CW, Szostak JW (2006) Telomeres and telomerase: The path from maize, Tetrahymena and yeast to human cancer and aging. Nat Med 12: 1133-1138.

25. Fisher JL, Schwartzbaum JA, Wrensch M, Wiemels JL (2007) Epidemiology of brain tumors. Neurol Clin 25: 867-890.

26. Tiwari SB, Amiji MM (2006) A review of nanocarrier-based CNS delivery systems. Curr Drug Deliv 3: 219-232.

27. Cuddapah VA, Robel S, Watkins S, Sontheimer H (2014) A neurocentric perspective on glioma invasion. Nat Rev Neurosci 15: 455-465.

28. Stupp R, Hegi ME, Mason WP, van den Bent MJ, Taphoorn MJ, et al. (2009) Effects of radiotherapy with concomitant and adjuvant temozolomide versus radiotherapy alone on survival in glioblastoma in a randomized phase III study: 5-year analysis of the EORTC-NCIC trial. Lancet Oncol 10: 459-466.

29. Faivre S, Djelloul S, Raymond E (2006) New paradigms in anticancer therapy: Targeting multiple signaling pathways with kinase inhibitors. Semin Oncol 33: 407-420.

30. Valable S, Barbier EL, Bernaudin M, Roussel S, Segebarth C, et al. (2008) In vivo MRI tracking of exogenous monocytes/macrophages targeting brain tumors in a rat model of glioma. NeuroImage 40: 973-983.

31. Sturm D, Bender S, Jones DT, Lichter P, Grill J, et al. (2014) Paediatric and adult glioblastoma: Multiform (epi)genomic culprits emerge. Nat Rev Cancer 14: 92-107.

32. Ransohoff RM, Perry VH (2009) Microglial physiology: unique stimuli, specialized responses. Annu Rev Immunol 27: 119-145.

33. Watters JJ, Schartner JM, Badie B (2005) Microglia function in brain tumors. J Neurosci Res 81: 447-455.

34. Banerjee S, Bhat MA (2007) Neuron-glial interactions in blood-brain barrier formation. Annu Rev Neurosci 30: 235-258.

35. Zhai H, Heppner FL, Tsirka SE (2011) Microglia/macrophages promote glioma progression. Glia 59: 472-485.

36. Tambuyzer BR, Ponsaerts P, Nouwen EJ (2009) Microglia: Gatekeepers of central nervous system immunology. J Leukoc Biol 85: 352-370.

37. Voisin P, Bouchaud V, Merle M, Diolez P, Duffy L, et al. (2010) Microglia in close vicinity of glioma cells: Correlation between phenotype and metabolic alterations. Front Neuroenergetics 2: 131.

38. Hanisch UK, Kettenmann H (2007) Microglia: Active sensor and versatile effector cells in the normal and pathologic brain. Nat Neurosci 10: 1387-1394.

39. Xiong A, Yang Z, Shen Y, Zhou J, Shen Q (2014) Transcription Factor STAT3 as a Novel Molecular Target for Cancer Prevention. Cancers (Basel) 6: 926-957.

40. Bishop JL, Thaper D, Zoubeidi A (2014) The Multifaceted Roles of STAT3 Signaling in the Progression of Prostate Cancer. Cancers (Basel) 6: 829-859.

41. Boland ML, Chourasia AH, Macleod KF (2013) Mitochondrial dysfunction in cancer. Front Oncol 3: 292.

42. Malumbres M, Barbacid M (2009) Cell cycle, CDKs and cancer: A changing paradigm. Nat Rev Cancer 9: 153-166.

43. Lee R, Kim IS, Han N, Yun S, Park KI, et al. (2014) Real-time discrimination between proliferation and neuronal and astroglial differentiation of human neural stem cells. Sci Rep 4: 6319.

44. Besson A, Dowdy SF, Roberts JM (2008) CDK inhibitors: Cell cycle regulators and beyond. Dev Cell 14: 159-169.